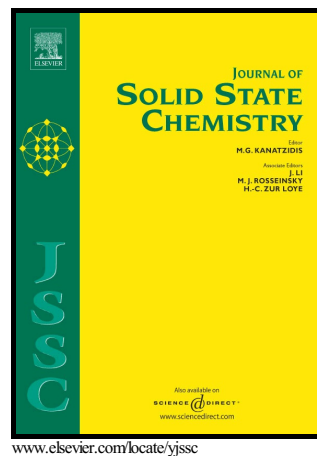


Author's Accepted Manuscript

Low temperature magneto-structural transitions in
 $Mn_3Ni_{20}P_6$

J. Cedervall, P. Beran, Marie Vennström, Therese Danielsson, Sabina Ronneteg, Viktor Höglin, David Lindell, O. Eriksson, G. André, Y. Andersson, P. Nordblad, M. Sahlberg



PII: S0022-4596(16)30053-6

DOI: <http://dx.doi.org/10.1016/j.jssc.2016.02.028>

Reference: YJSSC19275

To appear in: *Journal of Solid State Chemistry*

Received date: 16 December 2015

Revised date: 17 February 2016

Accepted date: 18 February 2016

Cite this article as: J. Cedervall, P. Beran, Marie Vennström, Therese Danielsson, Sabina Ronneteg, Viktor Höglin, David Lindell, O. Eriksson, G. André, Y. Andersson, P. Nordblad and M. Sahlberg, Low temperature magneto-structural transitions in $Mn_3Ni_{20}P_6$, *Journal of Solid State Chemistry* <http://dx.doi.org/10.1016/j.jssc.2016.02.028>

This is a PDF file of an unedited manuscript that has been accepted for publication. As a service to our customers we are providing this early version of the manuscript. The manuscript will undergo copyediting, typesetting, and review of the resulting galley proof before it is published in its final citable form. Please note that during the production process errors may be discovered which could affect the content, and all legal disclaimers that apply to the journal pertain

Low temperature magneto-structural transitions in $Mn_3Ni_{20}P_6$.

J. Cedervall¹, P. Beran², Marie Vennström³, Therese Danielsson⁴, Sabina Ronneteg³, Viktor Höglin⁵, David Lindell⁶, O. Eriksson⁷, G. André⁸, Y. Andersson¹, P. Nordblad⁹, M. Sahlberg¹

¹ Department of Chemistry - Ångström Laboratory, Uppsala University, Box 538, SE-751 21 Uppsala, Sweden

² Nuclear Physics Institute, ASCR, Hlavni 130, 25068 Rez, Czech Republic

³ AB Sandvik Materials Technology, SE-811 81, Sandviken, Sweden

⁴ Etteplan Sweden AB, SE-171 54 Solna, Sweden

⁵ Scienta Sauna Systems AB, SE-752 28, Uppsala, Sweden

⁶ Swerea KIMAB AB, Box 7047, SE-164 07, Kista, Sweden

⁷ Department of Physics and Astronomy, Uppsala University, Box 516, 751 20 Uppsala, Sweden

⁸ LLB, CEA-Saclay, 91191 Gif-sur-Yvette Cedex, France

⁹ Department of Engineering Sciences, Uppsala University, Box 534, 751 21 Uppsala, Sweden

Abstract

X-ray and neutron powder diffraction has been used to determine the crystal and magnetic structure of $Mn_3Ni_{20}P_6$. The crystal structure can be described as cubic with space group $Fm\bar{3}m$ (225) without any nuclear phase transformation within studied temperature interval from room temperature down to 4 K.

The magnetic structure of $Mn_3Ni_{20}P_6$ is complex with two independent magnetic positions for the Mn atoms and the compound passes three successive magnetic phase transitions during cooling. At 30 K the spins of the Mn atoms on the Wyckoff 4a site (Mn1) order to form a primitive cubic antiferromagnetic structure with propagation vector $\mathbf{k} = (0\ 0\ 1)$. Between 29 and 26 K the Mn atoms on the Wyckoff 8c site (Mn2) order independently on already ordered Mn1 magnetic structure forming a commensurate antiferromagnetic structure with propagation vector $\mathbf{k} = (0\ 0\ \frac{1}{2})$ and below 26 K, both Mn positions order to form an incommensurate helical structure with propagation vector $\mathbf{k} = (0\ 0\ \sim 0.45)$.

Magnetization vs. temperature curve of $Mn_3Ni_{20}P_6$ shows a steep increase indicating some magnetic ordering below 230 K and a sharp field dependent anomaly in a narrow temperature range around 30 K.

Keywords: Mn-compounds, magnetic structure, antiferromagnetism, neutron diffraction

Introduction

Manganese compounds often exhibit a complex magnetic behavior, for reasons which are not yet fully understood. This issue has e.g. been addressed by Eriksson *et al.* in a series of investigations of such systems [1, 2]. Compounds with the general formula Mn_3AB (A = Ir or Co, B = Si or Ge) have crystal structures very similar to that of the β -modification of elemental manganese, but in contrast to β -Mn an ordering of the magnetic Mn moments in a 120° spin

structure occurs at low temperature. This structure results from geometrical frustration of the antiferromagnetic interaction in a three-dimensional network of corner sharing Mn triangles [3]. For these types of compounds, the unit cell volume is important in determining the magnitude of the magnetic moment and the magnetic transition temperature, T_c ; both of which decreases with decreasing cell volume. Another interesting example is the compound IrMnSi which has a non-collinear magnetic structure with an incommensurate double cycloidal magnetic structure below 460 K [4].

In contrast to the antiferromagnetic compounds mentioned above, the magnetic structure of $Mn_3Pd_{20}P_6$ is ferromagnetic below 110 K [5], with a cubic $Fm\bar{3}m$ crystal structure. Its magnetic structure involves parallel moments on the two different crystallographic Mn sites, but with different magnetic moments. To further study the influence of the crystal structures on magnetic structures and properties, it is of interest to also determine the magnetic structure of the isostructural $Mn_3Ni_{20}P_6$. Keimes et al. [6] have reported $Mn_3Ni_{20}P_6$ to have an ordered $Cr_{23}C_6$ -type structure. In this paper, we report on the investigation of the (nuclear and) magnetic structure of $Mn_3Ni_{20}P_6$, characterized with powder neutron diffraction.

Experimental

Sample synthesis

Samples of composition $Mn_3Ni_{20}P_6$ were synthesized in a high frequency induction furnace with 300 mbar argon atmosphere. Pieces of manganese metal (Cerac, claimed purity 99.99 %, purified from manganese oxide by sublimation) and lumps of red phosphorus were dropped into a melt of nickel (Ni rods 99.995 %, Johnson and Matthey), as described by Rundqvist [7]. The compounds were annealed in evacuated silica tubes at 600°C for seven days.

X-ray diffraction

Phase analysis and unit cell determination was performed using a Guinier-Hägg powder diffraction camera with $CuK\alpha_1$ radiation and Si ($a = 5.43088 \text{ \AA}$, $T = 20^\circ\text{C}$) as internal calibration standard. Diffraction intensities were measured with a linear position sensitive detector (PSD) on a STOE & CIE GmbH STADI transmission X-ray powder diffractometer.

Neutron diffraction

Neutron powder diffraction data were collected at the G4-1 Cold Neutron Two-Axis Diffractometer at LLB in Saclay, France, for temperatures from 4 K to 300 K. The measurements were performed in the 2θ -range $3\text{--}82.9^\circ$ in steps of 0.10° . The sample was placed in a vanadium cylinder. The diffractometer was equipped with a vertical focusing pyrolytic graphite monochromator, giving a neutron wavelength of 2.42 \AA . Additional data were collected using the MEREDIT diffractometer at the Nuclear Physics Institute ASCR in Rez, Czech Republic. The neutron beam was monochromatized by a copper mosaic monochromator (reflection 220) providing a neutron wavelength of 1.46 \AA . Samples were studied in a 2θ -range of $4\text{--}144^\circ$ with steps of 0.08° collected at the same temperatures as for the LLB data.

Magnetic structure refinement

Crystal and magnetic structure refinements were performed by the Rietveld method [8], using the program FullProf [9]. Irreducible representation analysis was performed by SARAh software [10] which gave magnetic space groups for all magnetic structures and also the possibility to refine the magnetic parameters without any additional constraints.

Joined refinements of the G4.1 and MEREDIT datasets were performed for the room temperature, 30 K, and 4 K measurements. Due to the fact that the Q range of the MEREDIT instrument is much larger than that of G4.1, this procedure improved the determination of the structural parameters of the nuclear phase; these parameters were used also in the refinements at other temperatures.

The peak shape for G4.1 data was described by the pseudo-Voigt function with small asymmetry and the background was modelled by interpolation between fixed points. Profile parameters for MEREDIT data were fixed to values in the IRF (Instrument Resolution File). Profile parameters in IRF were obtained by refinement of a SiO_2 standard sample using same monochromator setup.

Magnetic measurements

A Quantum Design MPMSXL 5T SQUID magnetometer was used for the magnetization measurements. The magnetization was recorded as a function of temperature in a constant field and as a function of field at constant temperature.

Results and discussion

The crystal structure was confirmed to be cubic $\text{Fm}\bar{3}\text{m}$ (225) and isostructural with Cr_{23}C_6 , with cell parameter $a = 11.0820(2)$ Å at room temperature, in agreement with the results reported by Keimes *et al.* [6].

The crystal structure consists of two manganese positions called Mn1 and Mn2 with the Wyckoff positions $4a$ and $8c$ respectively. The Mn1 substructure is coordinated with 12 Ni atoms (cuboctahedron - MnNi_{12}) and 6 P atoms (octahedron - MnP_6) forming $\text{MnNi}_{12}\text{P}_6$ units centered in a face centered cubic lattice. The Mn atoms of the Mn2 substructure are coordinated with 4 Ni atoms (tetrahedron – MnNi_4) positioned at the tetrahedral positions of an fcc-lattice. The structure can thus be described as being of the CaF_2 -type where the calcium atoms correspond to the $\text{MnNi}_{12}\text{P}_6$ units and the fluorine atoms to the MnNi_4 units. In this way the crystal structure can be described as $\text{MnNi}_{12}\text{P}_6(\text{MnNi}_4)_2$, which has the correct composition, $\text{Mn}_3\text{Ni}_{20}\text{P}_6$, shown in Figure 1.

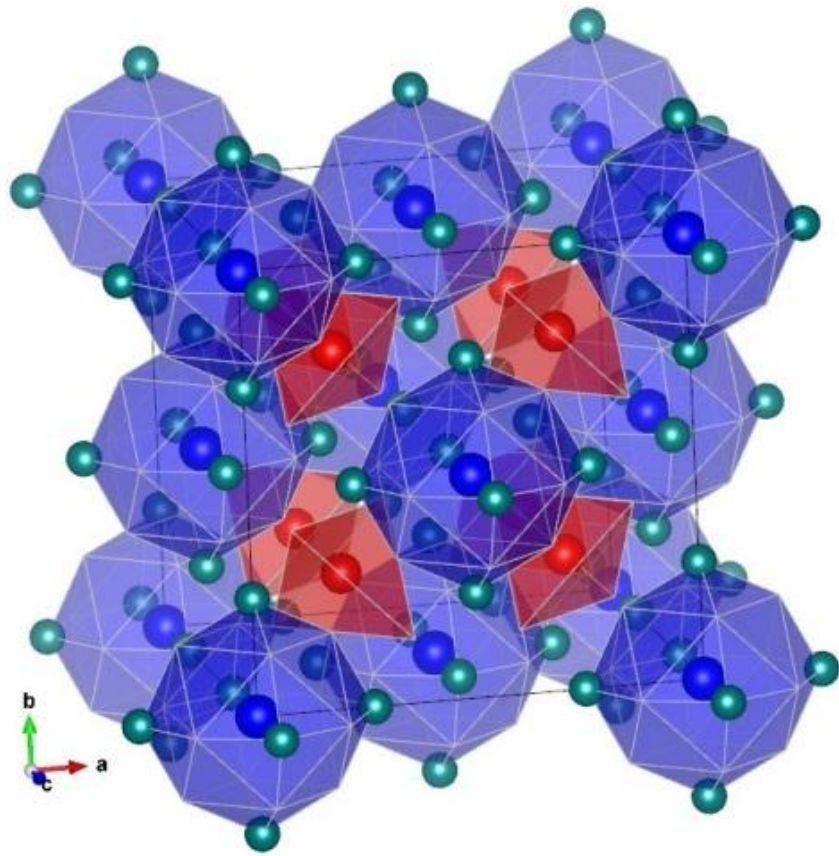


Figure 1 - Overview of the structure of $\text{Mn}_3\text{Ni}_{20}\text{P}_6$. The coordination of the Mn1 position is in blue, the coordination of the Mn2 position is in red, the phosphorus atoms are in green and the nickel atoms are not shown but they are situated at the empty corners of the polyhedra.

Magnetization measurements

Earlier magnetization experiments indicate that $\text{Mn}_3\text{Ni}_{20}\text{P}_6$ orders magnetically in an antiferromagnetic (or weakly ferrimagnetic) structure below ~ 240 K [5]. There exists however an excess (very weak) ferromagnetic moment already at higher temperatures – possibly emanating from a magnetic impurity phase (< 1%) unresolved by XRPD and NPD. At about 30 K there is a sharp and narrow field dependent anomaly in the magnetization vs temperature curve (Figure 1a) and a distinctly altered M vs. H behavior with a temperature dependent step like feature (Figure 1b). This low temperature behavior reflects the structural changes revealed by our NPD experiments as discussed in the following section.

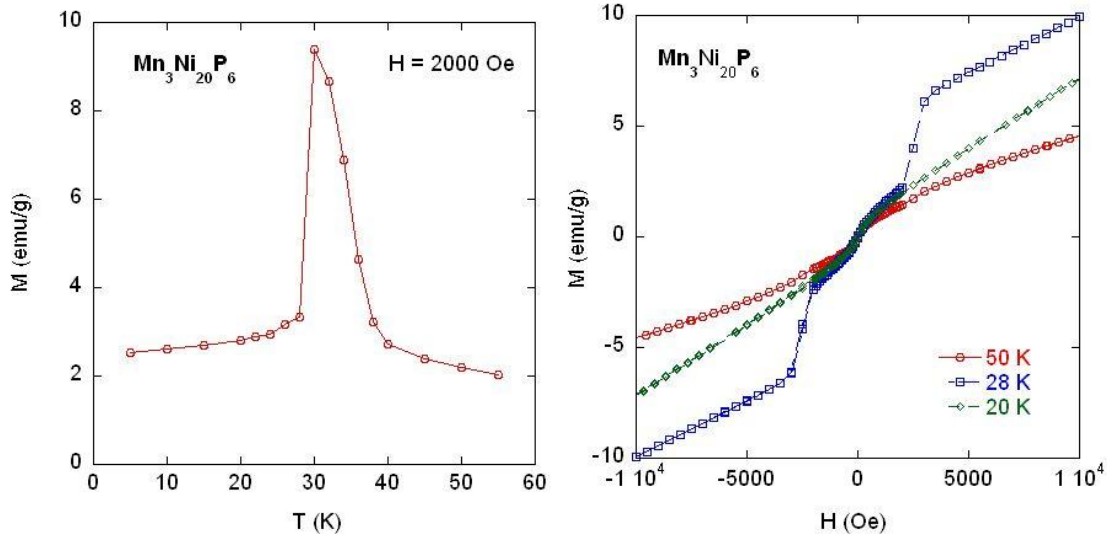


Figure 2 - Left, low temperature dependence of the magnetization measured in the magnetic field of 2000 Oe. Right, magnetization vs. magnetic field measured at 20, 28 and 50 K.

Magnetic structure

$\text{Ni}_{20}\text{Mn}_3\text{P}_6$ passes through several magnetic transformations during cooling. There exist two Mn-positions with different coordination that independently orders magnetically with different moments and spin arrangements. From the neutron diffraction patterns three different magnetic arrangements were found (see Figure 3), which are described in details in the following.

Magnetic structure at 30K

On the neutron diffraction patterns at 30 K only small additional reflections at $Q = 0.56$ and 1.39 \AA^{-1} were found (see Figure 3). They can be indexed within the magnetic structure CAmca where only atoms of Mn1-position (blue in Figure 1) are ordered with propagation vector $\mathbf{k} = (0\ 0\ 1)$. Measured and refined neutron diffraction pattern at 30 K are shown in Figure 4.

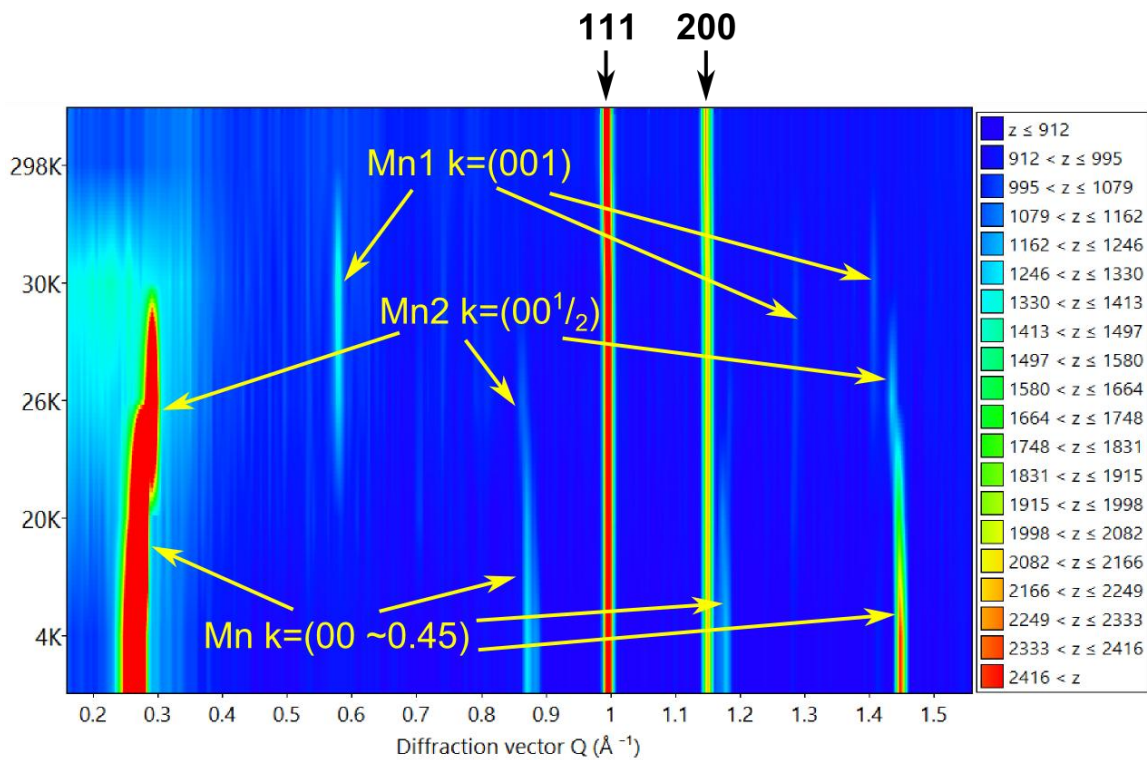


Figure 3 - Intensity color map of the low angle portion of the neutron diffraction patterns of G4.1. Nuclear reflections are marked as well as the magnetic reflections of three different magnetic arrangements as they evolve with temperature (y axis).

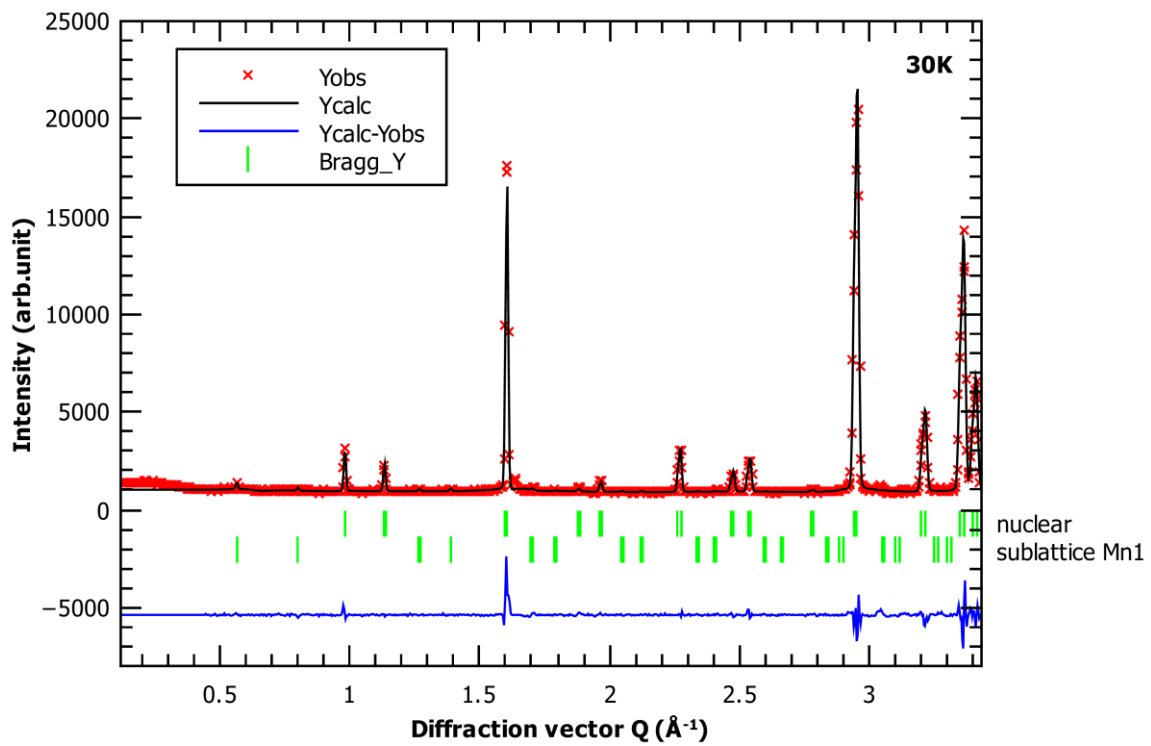


Figure 4 - Measured and calculated G4.1 neutron diffraction pattern at 30 K. Individual Bragg contributions of nuclear and magnetic phase are shown.

Analysis of the measured data reveals that the magnetic moments are arranged ferromagnetically in the ab -plane and these planes are regularly coupled antiferromagnetically along the c -direction as shown in Figure 5.

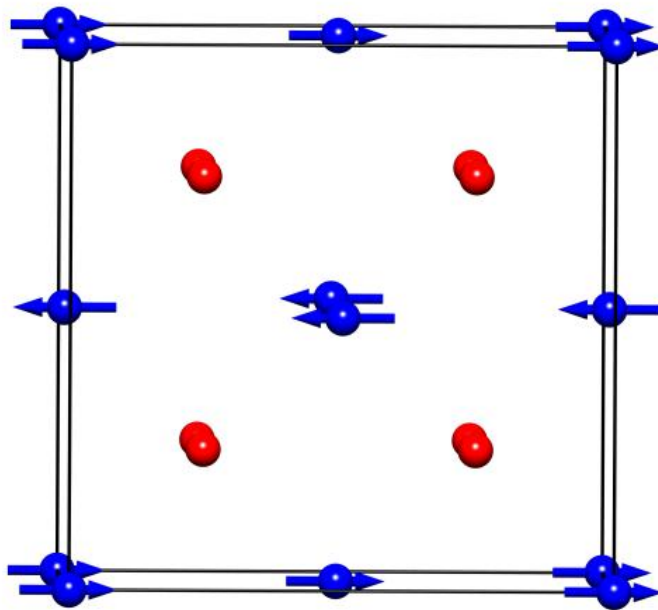


Figure 5 – Graphical representation of magnetic arrangement of the Mn1-position at 30 K. Blue balls represent Mn1, that are carry a magnetic moment at 30 K. Red balls represent Mn2-positions, that does not carry a magnetic moment at this temperature.

Commensurate magnetic structure 26 – 29 K

When the temperature is reduced from 30 K, the Mn atoms at the Mn2 position starts to order without disturbing the Mn1, and a new commensurate magnetic structure, $Cm'm2'$, is present between 26 and 29 K. On the neutron diffraction pattern another set of reflections appear from the ordering at Mn2 (see Figure 6). The atomic moments on Mn2 are arranged antiferromagnetically with propagation vector of $\mathbf{k} = (0\ 0\ \frac{1}{2})$. See Figure 7 for a graphical representation. In the c-direction there are ferromagnetically coupled ab layers stacked as follow 2/-1/2/-3/2/-1/2/-3/..., where negative sign means antiferromagnetic ordering.

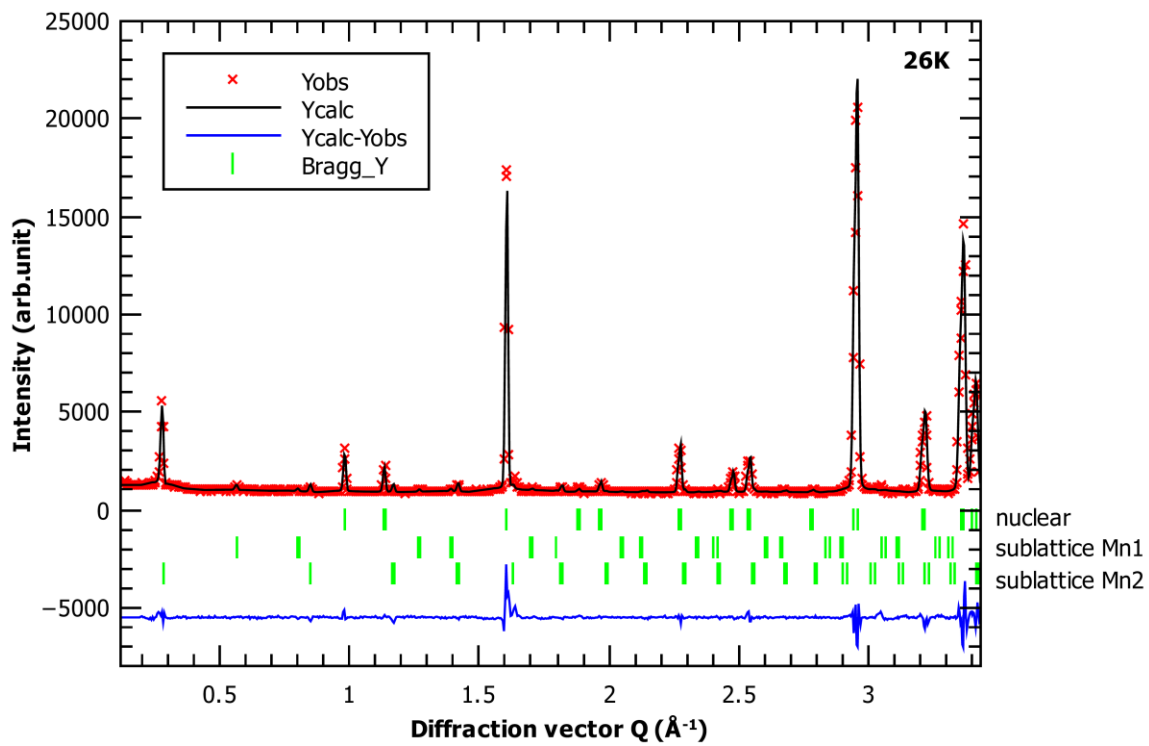


Figure 6 - Measured and calculated G4.1 neutron diffraction pattern at 26 K. Individual Bragg contributions of nuclear and two magnetic phases are shown.

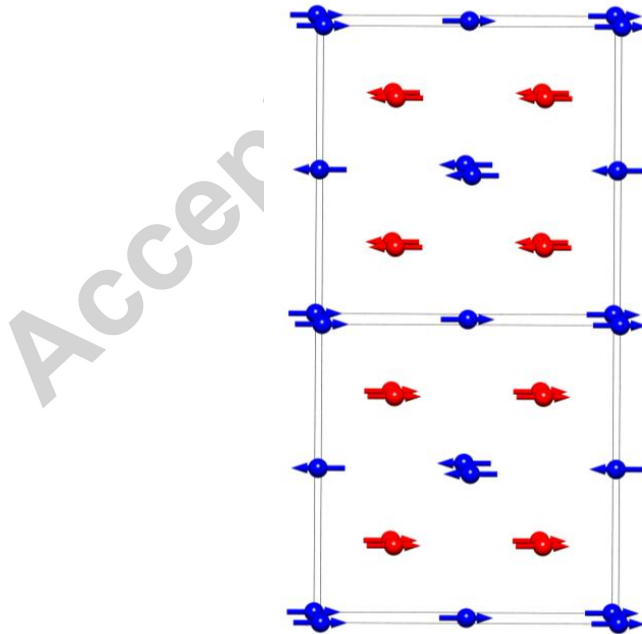


Figure 7 – Graphical representation of magnetic arrangement on both Mn1 (blue) and Mn2 (red) positions at 26 K. View along b axis.

Incommensurate magnetic structure, 4 – 25 K

The magnetic structure from 4-25 K is from the low temperature NPD patterns (see Figure 8 for data at 4 K) and is refined as an incommensurate helical structure along one of the crystallographic axes, within the magnetic space group $C_{\text{cm}}mc2_1$. It can be described by a propagation vector $k_{4\text{K}} = (0, 0, 0.4548(3))$. The magnetic moment of the manganese atoms in the two different crystallographic positions are at 4 K determined to be $4.3(3)$ and $4.7(1) \mu_{\text{B}}$ for site 4a and 8c, respectively. The derived magnetic structure is illustrated in Figure 9; blue arrows Mn1 and red arrows Mn2. By decreasing the temperature within this interval (25 – 4 K) the magnetic moments on both sites increased but the value of propagation vector decreases. Summary of all calculated magnetic moments and propagation vectors together with R-factors are listed in Table 1.

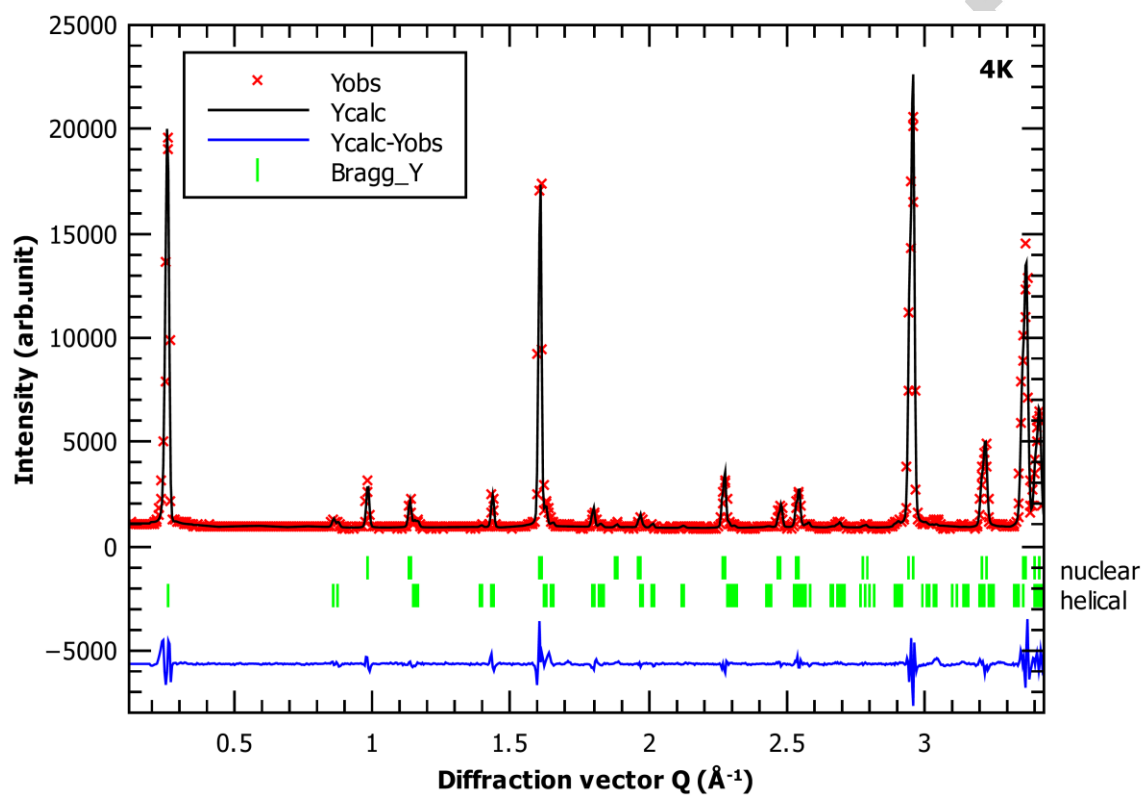


Figure 8 - Measured and calculated G4.1 neutron diffraction pattern at 4 K. Individual Bragg contributions of nuclear and two magnetic phases are shown.

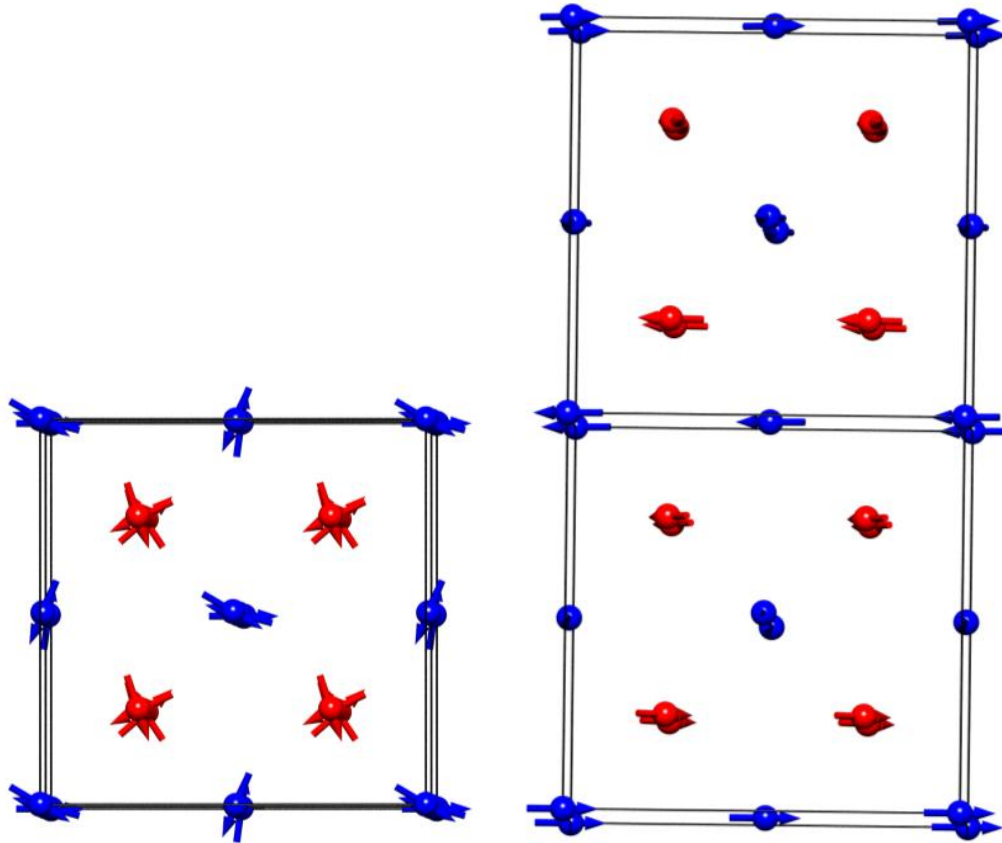


Figure 9 – Graphical representation of incommensurate helical magnetic structure at 4 K (propagation vector $\mathbf{k} = (0 0 \sim 0.45)$). Left view along c -axis and right view along b -axis.

Table 1 - Summary of parameters of magnetic arrangement for $\text{Ni}_{20}\text{Mn}_3\text{P}_6$ for different temperatures. R_{mag} values for the $\mathbf{k}_1 = (0 0 1)$ model are very high due to very low observed magnetic intensities and should not be considered reliable.

Temperature	30 K	26 K	20 K	4 K
4a site, Mn1	$\mathbf{k}_1 = (0 0 1)$	$\mathbf{k}_1 = (0 0 1)$	$\mathbf{k}_3 = (0 0 0.4635(3))$	$\mathbf{k}_3 = (0 0 0.4548(3))$
8c site, Mn2	–	$\mathbf{k}_2 = (0 0 1/2)$	–	–
4a site, \mathbf{k}_1	$2.4(2) \mu_B$	$2.2(3) \mu_B$	–	–
8c site, \mathbf{k}_2	–	$2.7(2) \mu_B$	–	–
4a site, \mathbf{k}_3	–	–	$3.6(4) \mu_B$	$4.3(3) \mu_B$
8c site, \mathbf{k}_3	–	–	$3.4(2) \mu_B$	$4.7(1) \mu_B$
R_{Bragg}	3.12	3.34	3.62	3.97
R_{mag}	(55)	(38)/14.2	12.8	9.9

A similar behavior with independent antiferromagnetic ordering on the two magnetic positions at low temperatures has been observed for isostructural compounds of the general formula $\text{RE}_3\text{Ni}_{20}\text{X}_6$ (RE = rare earth element, X = Ge, Si)[11-14]. There are however only two other examples showing three successive magnetic phase transitions [11, 15] and it is argued to depend on sample quality and homogeneity what type of magnetic behavior is observed.

However, the magnetic ordering in $RE_3Ni_{20}X_6$ -type compounds occurs typically at lower temperatures (below 10 K) than in $Mn_3Ni_{20}P_6$. Another difference between $Mn_3Ni_{20}P_6$ and $RE_3Ni_{20}X_6$ is that in former case the magnetic atoms on the 4a site (i.e. Mn1) order first whereas in the latter case the magnetic atoms on the 8c site (i.e. Mn2) order first.

Given the complex behavior of the magnetic ordering in this system, further investigations, in combination with theory, are needed to fully elucidate the magnetic interactions in $Mn_3Ni_{20}P_6$.

$Mn_3Ni_{20}P_6$ and the similar compound $Mn_3Pd_{20}P_6$ are isostructural but have different magnetic behavior, although, in both compounds the magnetic properties can be assigned to the Mn-atoms. The distances between the magnetic Mn-atoms are however different in the two systems which are why the magnetic coupling mechanisms are different, where the $Mn_3Pd_{20}P_6$ orders ferromagnetically, and $Mn_3Ni_{20}P_6$ have the complex antiferromagnetic structure discussed above. Deeper discussions between these compounds can be found in Eriksson et. al. [5].

Summary and conclusions

The magnetic structure of $Mn_3Ni_{20}P_6$ has been determined to be strongly dependent on the temperature. At higher temperatures (above 30 K), the Mn1 positioned atoms order with a $\mathbf{k} = (0\ 0\ 1)$ propagation vector, while the Mn2 position is disordered. This shows that the strongest exchange interaction in this system is coming from the Mn1 positions. Upon cooling (26-29 K) the Mn-atoms in the Mn2-positions also orders, resulting in a collinear but complex antiferromagnetic structure with a $\mathbf{k} = (0\ 0\ \frac{1}{2})$ propagation vector. Upon further cooling (4-25 K) a non-collinear magnetic state develops, with propagation vector $\mathbf{k} = (0,\ 0,\ \sim 0.45)$. It is tempting to associate these two transitions with a hierarchy of interactions in which the interactions from the Mn2-positions are stronger than the interactions between the Mn1 and Mn2 positions. However, more complex sets of interactions between the different atomic positions may be envisioned, and possibly finite temperature effects of the exchange interactions themselves [16] might play role. Hence, the complex set of interactions among Mn atoms, as evidenced in this study, calls for a theoretical first principles investigation and we hope our work will stimulate such theories.

Acknowledgement

Financial support from the Swedish Research Council and the KAW foundation is gratefully acknowledged. PB acknowledges support from CANAM infrastructure (MSMT project no. LM2011019) and NMI3-II project (grant no. 283883).

References

[1] T. Eriksson, L. Bergqvist, P. Nordblad, O. Eriksson, Y. Andersson, *Journal of Solid State Chemistry* 177 (2004) 4058-4066.

[2] T. Eriksson, R. Lizárraga, S. Felton, L. Bergqvist, Y. Andersson, P. Nordblad, O. Eriksson, *Physical Review B* 69 (2004) 054422.

[3] T. Eriksson, L. Bergqvist, Y. Andersson, P. Nordblad, O. Eriksson, *Physical Review B* 72 (2005) 144427.

[4] T. Eriksson, L. Bergqvist, T. Burkert, S. Felton, R. Tellgren, P. Nordblad, O. Eriksson, Y. Andersson, *Physical Review B* 71 (2005) 174420.

[5] T. Eriksson, M. Vennström, S. Ronneteg, Y. Andersson, P. Nordblad, *Journal of Magnetism and Magnetic Materials* 308 (2007) 203-209.

[6] V. Keimes, A. Mewis, *Zeitschrift fur anorganische und allgemeine Chemie* 618 (1992) 35-38.

[7] S. Rundqvist, *Chemica Scripta* 28 (1988) 15-20.

[8] H.M. Rietveld, *Journal of Applied Crystallography* 2 (1969) 65-71.

[9] J. Rodríguez-Carvajal, *Physica B: Condensed Matter* 192 (1993) 55-69.

[10] A.S. Wills, *Physica B: Condensed Matter* 276-278 (2000) 680-681.

[11] A. Dönni, F. Fauth, P. Fischer, T. Herrmannsdörfer, L. Keller, T. Komatsubara, *Journal of Alloys and Compounds* 306 (2000) 40-46.

[12] J. Kitagawa, N. Takeda, M. Ishikawa, *Journal of Alloys and Compounds* 256 (1997) 48-56.

[13] T. Herrmannsdörfer, A. Dönni, P. Fischer, L. Keller, H. Kitazawa, *Physica B: Condensed Matter* 281-282 (2000) 167-168.

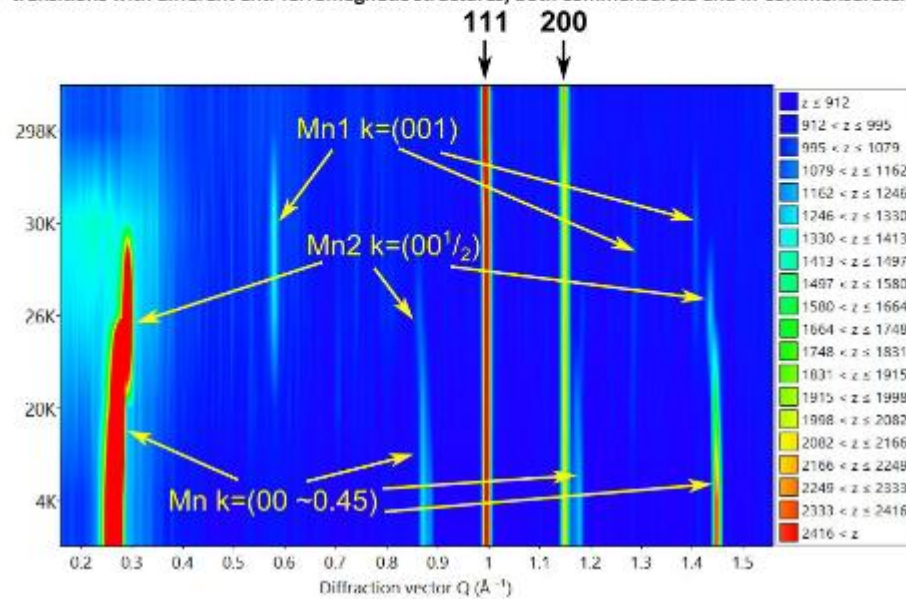
[14] T. Herrmannsdörfer, A. Dönni, P. Fischer, L. Keller, G. Böttger, M. Gutmann, H. Kitazawa, J. Tang, *Journal of Physics: Condensed Matter* 11 (1999) 2929.

[15] A. Dönni, L. Keller, P. Fischer, Y. Aoki, H. Sato, F. Fauth, M. Zolliker, T. Komatsubara, Y. Endoh, *Journal of Physics: Condensed Matter* 10 (1998) 7219.

[16] A. Szilva, M. Costa, A. Bergman, L. Szunyogh, L. Nordström, O. Eriksson, *Physical Review Letters* 111 (2013) 127204.

Graphical abstract

$\text{Mn}_3\text{Ni}_{10}\text{P}_6$ has been investigated using neutron diffraction and undergoes several magnetic transitions with different anti-ferromagnetic structures, both commensurate and in-commensurate.



Graphical abstract

Mn₃Ni₂₀P₆ has been investigated using neutron diffraction and undergoes several magnetic transitions with different anti-ferromagnetic structures, both commensurate and in-commensurate.

Highlights

The crystal and magnetic structure have been determined by XRD and NPD.
At 30 K the spin on Mn1 order and forms an antiferromagnetic structure.
Between 29 and 26 K the Mn2 also orders antiferromagnetically.
Below 26 K all Mn atoms orders in an incommensurate helical structure.

Accepted manuscript